Check for updates

Structural arrest and dynamic localization in biocolloidal gels†

N. Mahmoudi [ID] ‡*[ab] and A. Stradner [ID] *[b]

Casein micelles interacting *via* an entropic intermediate-ranged depletion attraction exhibit a fluid-to-gel transition due to arrested spinodal decomposition. The bicontinuous networked structure of the gel freezes shortly after formation. We determine the timescales of structural arrest from the build-up of network rigidity after pre-shear rejuvenation, and find that the arrest time as well as the plateau elastic modulus of the gel diverge as a function of the volume fraction and interaction potential. Moreover, we show using scaling from naïve mode coupling theory that their mechanical properties are dictated by their microscopic dynamics rather than their heterogeneous large scale structure.

Introduction

Gels are disordered solid-like materials with unique structural and mechanical properties.[1] They are found in numerous industrial and biological applications such as 3D printing inks,[2] templates for porous materials,[3] food formulations[4] and in biomedicine as tissue scaffolds and molecule delivery carriers.[5,6] Their mechanisms of formation in colloidal suspensions has attracted ample attention from a fundamental viewpoint[7,8] and also because of their relevance to applications.[9,10]

While most of the early studies on colloid phase transitions of the last three decades reported either on diffusion-limited cluster aggregation (DLCA) gels at very low volume factions, ϕ,[11] or on glasses at large ϕ,[12] the more recent ones have focused on elucidating the fundamental mechanisms of gelation at intermediate ϕ. For example, in thermo-reversible adhesive hard spheres (AHS)[13,14] and nanoemulsions,[15,16] gelation proceeds either due to homogeneous percolation or *via* arrested phase separation, depending on ϕ. Very recently, Hsiao and Doyle demonstrated the coexistence of percolation and arrested phase separation in thermo-gelation of nanoemulsions over a broad range of ϕ and temperatures.[17] In contrast, arrested spinodal decomposition has lately garnered consensus as the gelation mechanism in depletion systems,[18–22] and also in other systems such as lysozyme with temperature-dependent attractions[23] and thermo-responsive silica particles.[24] As such, gelation occurs

when the system phase-separates into colloid-rich and colloid-poor regions and then becomes arrested due to an attractive glass transition in the colloid-rich region.[1]

Gelation *via* spinodal decomposition has been shown to strongly depend on the range of the attraction potential, relative to the particle diameter, δ. For colloidal systems with short-range attractions, $\delta \lesssim 0.1$, the fluid-to-gel transition coincides with the metastable fluid–fluid spinodal.[18,25–27] For longer-range systems, $\delta \gtrsim 0.3$, the gelation transition is off-set with respect to the spinodal boundary,[28,29] *i.e.* the system shows a gradual change from phase separation to gelation as a function of the quench depth.[29,30] Nevertheless, gelation in systems with intermediate-to-long range attraction was also shown to occur in the immediate vicinity of the phase separation boundary, indicating that gelation proceeds *via* arrest of spinodal decomposition.[31,32]

Entwined with the argument about whether the transition from spinodal decomposition to gelation is direct or gradual is the debate about the structural coarsening or absence thereof in colloidal gels. Indeed recent experimental[28,29] and numerical studies[33] indicate that colloidal gels with intermediate-to-long range attractions coarsen over long times after gelation. In contrast, several other experimental studies have shown that the structure of gels with short-ranged attraction arrests completely at some time after gelation.[1,18,23,24,26,31] However, this divide along the attraction range is not that clear cut as intermediate-range thermo-reversible colloidal gels have been shown to arrest shortly after they form[32] while short-range depletion gels have been shown to coarsen.[20]

Arrested phase-separated gels have been shown to age-stiffen and mechanisms abound as to what causes their elasticity increase with waiting time. On one hand, it has been suggested that coarsening drives depletion gels to stiffen with age.[34–36] On the other hand, Guo *et al.* have found a connection between the

[a] Adolphe Merkle Institute, University of Fribourg, Route de l'ancienne Papeterie 1, Marly, Switzerland. E-mail: najet.mahmoudi@stfc.ac.uk

[b] Physical Chemistry, Lund University, Getingevägen 60, Lund, Sweden. E-mail: anna.stradner@fkem1.lu.se

† Electronic supplementary information (ESI) available: Temporal evolution of rheological and dynamical properties of gels. See DOI: 10.1039/c7sm00496f

‡ Current address: ISIS Facility, STFC, Rutherford Appleton Lab., Harwell Science & Innovation Campus, Didcot, OX11 0QX, UK.

age-dependence of rheological behaviour and that of particle dynamics of thermo-reversible gels with short-ranged attractions.[24] This connection was made through mode coupling theory whereby the localization length which defines particle caging correlates with a growing elastic modulus.[37] In contrast, Zia *et al.* have shown that the effect of this pair-level relaxation on gel elasticity is secondary and that it is rather relaxation at larger length scales that primarily drives age stiffening in short-range colloidal gels.[20]

In this work we explore several of the above issues in a polydisperse biocolloidal system where casein micelles form a gel *via* a polymer-induced depletion attraction and through an arrested spinodal decomposition mechanism. We show using a time-dependence characterization of the structure and mechanics of the gel network that the structural arrest occurs within the early stages of gel formation, and that the plateau elastic modulus exhibits a power-law divergence as a function of the casein volume fraction, ϕ, and the depletion potential, U. We successfully connect the elastic shear modulus to the casein localization length through naïve mode coupling theory, and extend its applicability to the kinetics of gel formation.

Experimental

Our system consists of polydisperse casein micelles (ref. MPI-85 MC, Hungarian Institute of Dairy Research) with a radius $R \approx 55$ nm and a polydispersity of 40%, and quasi-mono-disperse polyethylene oxide (PEO) from Polymer Source Inc. with a gyration radius of $R_g \approx 17$ nm and a molecular weight $M_w \approx 121$ kDa. Casein–PEO mixtures are made from stock solutions of casein and of PEO prepared in 100 mM NaCl as described in ref. 38. We follow the formation kinetics of casein-micelle gels by measuring their structure, dynamics and mechanical properties using confocal laser scanning microscopy (CLSM), diffusing-wave spectroscopy (DWS) and rheology, respectively.

CLSM measurements were performed on an inverted Leica TCS SP5 (DMI 6000 B) using a 63× glycerol–water immersion objective. Casein micelles were non-covalently labelled with Rhodamine B and loaded between a microscope slide and a cover slip using a Secure-Seal imaging spacer (Sigma, 120 μm thickness, window diameter 13 mm). 512 × 512 pixel-resolution images were acquired 10–15 μm from the cover slip to avoid wall effects and over a depth of 30–40 μm.

DWS measurements were done on a Rheolab (λ = 632.8 nm, LS Instruments, Switzerland) and on a home-built DWS setup[39] (50 mW single longitudinal mode diode laser, λ = 657 nm, CrystalLaser), both combining the two-cell technique[40] and the echo-technique.[41] The scattered light with a wave vector magnitude $k_0 = 2\pi n/\lambda$, with n the refractive index of the solvent, was detected in transmission by a mono-mode fiber, and analysed by a single-photon counter and a correlator. Measurements were done at different waiting times, t_w, after mixing at 22 °C in standard cuvettes with a 4 or 5 mm thickness, L. Polystyrene sulfonate particle ($2R \approx 460$ nm, Polysciences Inc.) suspensions with known photon transport mean free path, l^*, are used as a reference to determine the l^* of casein micelles.

Rheological properties were measured on a stress-controlled rheometer (AR-G2, TA Instruments) in double gap concentric cylinders geometry (rotor outer radius 17.5 mm, rotor inner radius 16 mm, stator inner radius 15.1 mm) at 22 °C. Samples were pre-sheared for 60 s at $\gamma = 1000$ s^{-1}, after loading, to ensure the same starting point for all samples.[42] The build-up of gel elasticity is measured in the linear regime at $\omega = 1$ rad s^{-1} and at a shear amplitude of $\gamma = 1\%$ as a function of t_w.

Results and discussion

Structural arrest

Fig. 1 summarizes the effects of an intermediate-ranged depletion attraction on the macroscopic solution behaviour of casein micelles. Shown is the state diagram as a function of the casein volume fraction, ϕ, and the strength of the effective depletion attraction potential, U, calculated using the generalized free volume theory (see details of the calculations in the ESI†).[43] The corresponding phase diagram as function of the reduced polymer concentration (c/c^*) is shown in Fig. S1 (ESI†). It demonstrates that casein micelles can transform from fluid structures to disordered solid states (Fig. 1). The gelation proceeds directly from the homogeneous fluid phase at $\phi \geq 0.3$, while at lower ϕ a continuous crossover from phase separation to gelation is observed. Marked features of the gel formation are the appearance of large length-scale heterogeneities (Fig. 2a) and the onset of an elastic mechanical response (Fig. 2d). In addition, the dynamics show a two-step decay, reflecting the increasingly restricted motion of casein micelles within the gel (Fig. 2b).

To gain insight into the network structural behaviour, we recorded 2D CLSM images of the structural evolution of the sample. The set of images in Fig. 2a illustrates the typical demixing kinetics for a relatively deep quench ($U \sim -9k_BT$). We see that the coarse spinodal domain structure initially formed
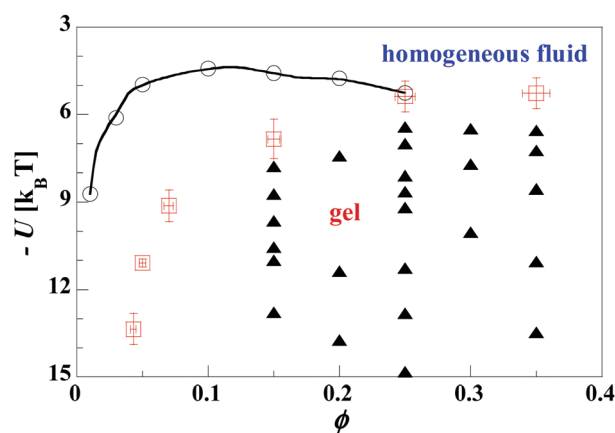

Fig. 1 Experimental state diagram for casein micelle–polyethylene oxide mixtures with polymer-to-colloid size ratio $\delta \approx 0.31$. Circles correspond to the fluid–fluid coexistence. Triangles correspond to gels studied in this work and determined by their rheology, dynamics and structural features as shown in Fig. 2. The solid line is a guide to the eye. Empty squares correspond to threshold ϕ, ϕ_g, and threshold U, U_g, determined from scaling rheology data along U- and ϕ-cuts.
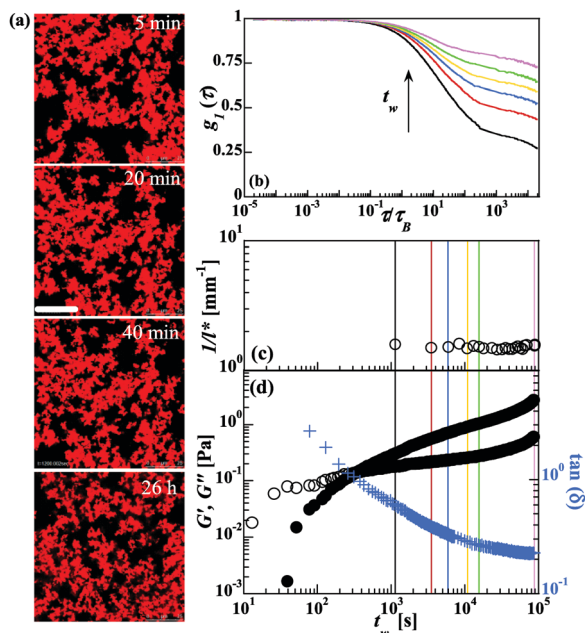
Fig. 2 Arrest of spinodal decomposition in a casein–PEO mixture at ϕ = 0.15 and $U \sim -9.6k_{\rm B}T$. (a) Time sequence of CLSM images of the gel formation. Scale bar represents 25 μm for all images. Casein network appears in red. (b) $t_{\rm w}$-Dependence of DWS intermediate scattering functions. The decay time τ is expressed in terms of the Brownian time $\tau_{\rm B}$. (c) Temporal evolution of the inverse of the photon transport mean free path, $1/l^*$. (d) Mechanical response as a function of $t_{\rm w}$ in the linear regime at ω = 1 rad s^{-1}: storage (solid circles), loss (open circles) moduli and $\tan(\delta) = G''/G'$ (plusses). The solid vertical lines in (c) and (d) mark the $t_{\rm w}$ at which the DWS $g_1(\tau)$ in (b) are measured.

is static, without any evidence of structural change during an imaging period of 2 days.

The structural evolution of the casein–PEO system of Fig. 2a is also determined from diffuse-transmission spectroscopy (DTS) measurements,[44] where structural properties of the system are extracted from DWS transmission measurements as detailed in ref. 38. For a suspension of hard spheres, l^* is related to the structural properties through:[45]

$$l^* = k_0^6 \left(\pi \rho \int_0^{2k_0} F(q) S(q) q^3 {\rm d}q \right)^{-1} \qquad (1)$$

with n the refractive index of the solvent, λ the wavelength of the laser, $\rho = \phi/(4\pi R^3/3)$ the particle number density, $q = 2k_0 \sin(\theta/2)$ the magnitude of the scattering vector, $F(q)$ the single-particle form factor, and $S(q)$ the structure factor. Using eqn (1), casein micelles were shown to behave, structurally, as hard spheres up to $\phi \approx 0.45$.[46]

In Fig. 2c and Fig. S2 in the ESI,† we confirm that the structural properties of the sample are unchanged, as shown by the $t_{\rm w}$-dependence of l^* during a DTS measurement period of 26 h. This structural arrest is reminiscent of colloidal systems interacting *via* short-to-medium range attraction,[18,23,31] where a solid-like gel forms due to spinodal decomposition into an interconnected colloid-rich network, followed by a local glass-like arrest of the dynamics.[21] Our results are consistent with

both numerical and experimental results of short-range attraction systems where structural arrest persists for two or more decades in time.[21,22]

Timescales of arrest from rheology

As the timescales of structural arrest turn out to be too fast to be captured by CLSM (sample preparation and loading of 5–10 min), we use temporal evolution of gel elasticity to extract them. Because of the strong shear-flow rejuvenating step (pre-shear at $\dot{\gamma}$ = 1000 s^{-1} after loading), the system exhibits liquid-like behaviour at short $t_{\rm w}$ (Fig. 2d), with the loss modulus G'' exceeding the storage modulus G'. Both moduli then increase rapidly with time, but G' rises faster than G'' such that there is a crossover at a characteristic time. This crossover time corresponds to the characteristic timescale for the structural arrest of the system after the perturbation induced by the pre-shear flow,[47] and is microscopically related to the timescale of dynamic arrest.[48] Examples of how this time depends on system parameters such as the volume fraction ϕ and the quench depth U are shown in Fig. S3a and b in the ESI,† respectively. This time ranged from about 10 to 500 s, with the shortest times encountered at the highest ϕ for a fixed U (Fig. S3a, ESI†) and for the deepest quench U at a constant ϕ (Fig. S3b, ESI†).

Following the approach of Rueb and Zukoski,[49] we determine the structural arrest time, $t_{\rm a}$, using an exponential approximation of the rise in G' at short-to-intermediate times:

$$G'(t_{\rm w}) = G_{\rm f}' \left(1 - \exp\left[-\Gamma_{\rm g}(t_{\rm w} - t_{\rm a})^\gamma \right] \right) \qquad (2)$$

where $\Gamma_{\rm g}$ is the growth rate of G' or rate of increase of gel connectedness, $G_{\rm f}'$ its plateau value, and γ is a stretched exponential coefficient.

Typical examples of the exponential growth of G' are displayed in Fig. 3a and b at three U values for ϕ = 0.15 and at three ϕ values and $U \approx -13k_{\rm B}T$, respectively. At long times, all systems assume a weak power-law growth $G' \sim t_{\rm w}^n$, with an exponent $n \approx 0.41 \pm 0.17$. The transition from exponential to
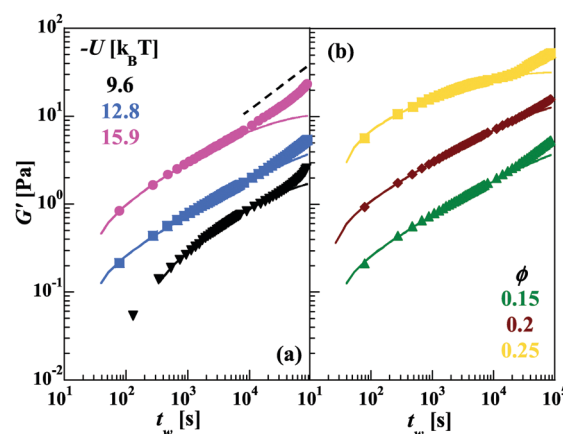

Fig. 3 Exponential growth of G' at short-to-intermediate times (solid lines) using eqn (1) at various U for ϕ = 0.15 (a), and at different ϕ for $U \approx -13 \pm 0.5k_{\rm B}T$ (b). For clarity, only three values of U (a) and ϕ (b) are shown. The dashed line shows the power-law growth of G' at long times.

power-law growth of G' along with the saturation of G''/G' (crosses in Fig. 2d) to a time-invariant value are indicative of two distinct processes.[24,42] The first is structural arrest and the second is aging.

We focus on the arrest timescales along several ϕ-cuts and U-cuts. We express them in terms of the Brownian relaxation time τ_B, the time for a casein micelle to diffuse its own radius by Brownian motion:

$$\tau_B = \frac{\pi \eta R^3}{k_B T} \qquad (3)$$

where η is the viscosity of the PEO solution in the free volume available to the polymer, as defined in ref. 43. τ_B varies between 0.4 and 2 μs.

In Fig. 4b and e, we plot t_a/τ_B as a function of the relative distance from the gel point $\phi^* = \phi/\phi_g - 1$ and $U^* = U/U_g - 1$, respectively. ϕ_g and U_g-values determined from rescaling U-cuts and ϕ-cuts (see details in the ESI†) are shown as red squares on Fig. 1. A critical-like dependence on both ϕ and U is observed, with a functional form:

$$t_a/\tau_B \propto U^{*-\nu_U} \left(\propto \phi^{*-\nu_\phi}\right) \qquad (4)$$

where $\nu_\phi \approx 1.9$ and $\nu_U \approx 2.7$. Likewise, a power-law divergence is found in the normalized growth rate $\Gamma_g \tau_B$:

$$1/\Gamma_g \tau_B \propto U^{*-\mu_U} \left(\propto \phi^{*-\mu_\phi}\right) \qquad (5)$$
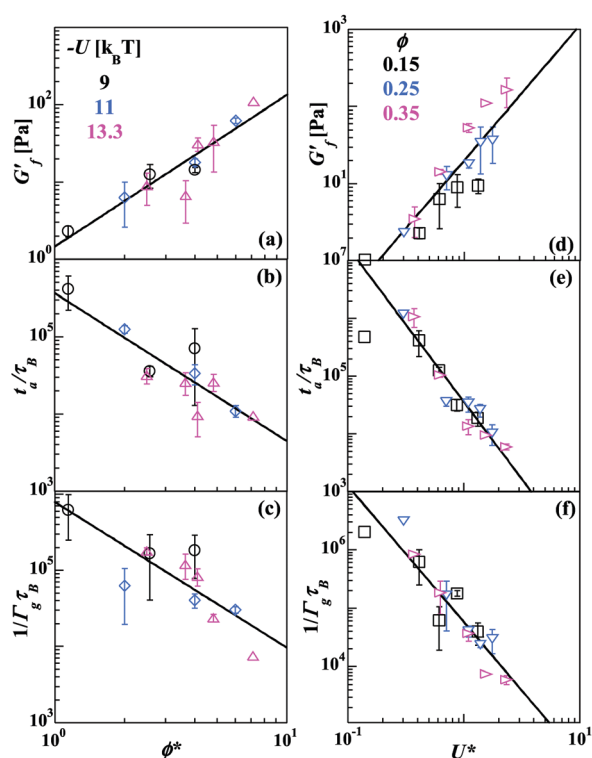

Fig. 4 Critical behaviour of the plateau elastic modulus (a and d), the normalized arrest time (b and e), and the normalized growth rate of G' (c and f), as a function of ϕ^* (left panels) and U^* (right panels). Solid lines are fits of scaled experimental data to eqn (6) on a and d, (4) on b and e, and (5) on c and f.

with $\mu_\phi \approx 1.9$ (Fig. 4c) and $\mu_U \approx 2.3$ (Fig. 4f). These results are similar to those of Guo *et al.* where a critical-like dependence of the arrest time and the growth rate on temperature is found for short-range interacting thermo-reversible silica nanoparticles.[24] They interpreted the timescale critical behaviour as reflecting the critical dynamics of spinodal decomposition, assuming that silica nanocolloids form gels through arrested spinodal decomposition.[24] t_a and Γ_g^{-1} were then inferred to reflect the duration of, respectively, the early and intermediate stages of spinodal decomposition, in analogy with *N*-isopropylacrylamide gels.[24,50] However, the lack of a rigorous microscopic interpretation of Γ_g, added to the impossibility of imaging the very first early times of the gel structure, prevents us from ascertaining that the gel structure arrests during the early stage of spinodal decomposition. We can thus only speculate that the structural arrest (at time t_a) occurs within the early stages of spinodal decomposition as in lysozyme solutions interacting *via* a short-range attraction.[51] It is interesting to note that in contrast to the deeply quenched gels studied here that undergo spinodal decomposition into a bicontinuous network with protein-rich and protein-poor domains, for gels with a shallow quench we initially do not observe the distinctive bicontinuous spinodal structure (see Fig. S5 in the ESI†). For shallow quenches we instead first find clusters of a few particle diameters, which coarsen into a bicontinuous spinodal structure, accompanied by a gradual transition from ergodic to non-ergodic dynamics. This seems to indicate that for these shallow quenches we are no longer in the bicontinuous spinodal decomposition regime, and that phase separation initially rather occurs *via* a nucleation and growth mechanism.

t_a values determined from rheology are significantly larger than percolation times of short-range depletion systems, t_p.[52] Indeed, Brownian dynamics (BD) simulations show that, at $0.15 < \phi < 0.3$, percolation is rapid and $\tau_B \lesssim t_p \lesssim 20\tau_B$.[52] We compare t_a values to estimates of the arrest time from fluid particle dynamics (FPD) simulations of short-range depletion system, and find that they are up to three orders of magnitude larger than the threshold time of $200\tau_B$ above which kinetic arrest occurs.[53] These estimations differ significantly from our experimental results, a discrepancy that could be ascribed to the incorporation of many-body hydrodynamic interactions in FPD simulations, while for our system, hydrodynamic interactions are screened because gels form at high polymer concentrations in the semi-dilute regime.[54]

Similarly to the gel's arrest time and growth rate, its plateau elastic modulus exhibits critical-like variation in both ϕ (Fig. 4a) and U (Fig. 4d):

$$G_f' \propto U^{*\nu_U} \left(\propto \phi^{*\nu_\phi}\right) \qquad (6)$$

In this case the critical exponents for the scaling of the experimental data are $\nu_\phi \approx 2$ and $\nu_U \approx 1.8$. This power-law divergence in the plateau modulus as a function of ϕ and U is reminiscent of the jammed systems[55] such as attractive colloidal gels,[49,56–58] and extends the critical behaviour in depletion gels to longer attraction range.[59] Furthermore, the critical exponent $\nu_\phi \approx 2$ is around the same value, $\nu_\phi \approx 2.1$, determined for

polymethyl-methacrylate/polystyrene (PMMA/PS) with $\delta \approx 0.18$, and significantly smaller than the value, $\nu_\phi \approx 3.3$, for short-range PMMA/PS, $\delta \approx 0.04$.[59]

It is worth noting that $\nu_\phi \approx 2$ is similar to values derived from examining fluid–solid transitions of thermo-reversible silica colloids as a function of time, with $\nu_\phi \approx 2$,[49,58] and $\nu_\phi \approx 1.7$.[57] The critical exponents are thus not universal but depend on the details of the interaction potential.

Scaling gel elasticity with casein localization

We have shown in the first and second parts of this section that while gel structure shows no coarsening on intermediate-to-long timescales, its elastic modulus increases exponentially before settling into power-law aging. In addition, the microscopic dynamics evolve rapidly with increasing t_w, as shown in intermediate scattering functions ($g_1(\tau)$) in Fig. 2b. For all $g_1(\tau)$'s, a two-step decay is observed, with a plateau separating the fast process, which increases with t_w, from a slow process that extends to longer times as t_w increases.

Two-step relaxations are a signature feature of the dynamics of a glass transition. Indeed, in colloidal suspensions near the glass transition, the particle dynamics separates into a fast/microscopic component in which a particle diffuses within the restricted cage of its neighbours, creating a partial decay in $g_1(\tau)$, and a slow/structural component in which the particle moves away from its cage with cooperative motion from its neighbours, leading to the final decay of $g_1(\tau)$. We thus interpret the microscopic partial decay of $g_1(\tau)$ of casein–PEO gels in terms of localized motion of the casein micelles within the cage of their neighbours. We determine the localization length of casein micelles by modelling $g_1(\tau)$'s with a stretched exponential:[60]

$$g_1(\tau) \cong \frac{(L/l^* + 4/3)\sqrt{k_0^2 \Delta^2 \left(1 - e^{-(\tau/\tau_f)^\beta}\right)}}{\sinh\left[(L/l^* + 4/3)\sqrt{k_0^2 \Delta^2 \left(1 - e^{-(\tau/\tau_f)^\beta}\right)}\right]} \quad (7)$$

with Δ the localization length, τ_f the fast relaxation time, and the stretched exponential coefficient decreasing from $\beta \approx 0.71$ to $\beta \approx 0.54$ with increasing t_w.

Examples of this subdiffusive motion in microscopic dynamics of casein–PEO gels are shown in Fig. 5 and Fig. S6 (ESI†). Such behaviour is qualitatively similar to that found in low-ϕ fractal as well as higher-ϕ colloidal gels.[61–64] The physical origin of this dynamics was found to be the internal elastic modes of many length scales of the gel, which was fully accounted for by the fractal model.[61] However, this fractal description relating microscopic dynamics and elastic properties of colloidal gels fails for $\phi > 0.1$ (details confirming its inapplicability to our system are in the ESI†).[64] We thus turn to naïve mode coupling theory (NMCT), which predicts power-law dependency of G' on ϕ in particle gels not based on the assumption of a fractal microstructure but as a result of ϕ dependence of δ. Here particle localization is predicted to be due to nearest neighbour crowding and inter-particle attractions. NMCT was recently applied by Schweizer *et al.* to relate the microscopic dynamics to
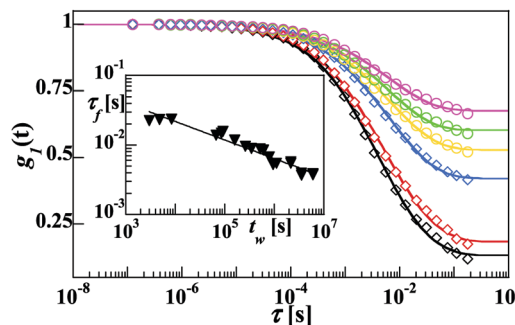

Fig. 5 DWS intermediate scattering functions, $g_1(\tau)$, as a function of t_w, increasing from bottom to top, for casein–PEO at $\phi = 0.15$ and $U \approx -13$, and the corresponding stretched-exponential decay fits (solid lines) using eqn (7). Inset: t_w-dependence of the fast relaxation time. The solid line is a power-law fit of the experimental data.

the mechanical properties of concentrated short-range attraction colloidal gels, using an exact relation between Δ and G',[37,65]

$$\frac{G'D^3}{k_B T} = \frac{9\phi D^2}{5\pi \Delta^2} \quad (8)$$

with D the diameter of the particles.

In Fig. 6 and 7, we show examples of Δ and G' scaled using, respectively, the right and left side of eqn (8), as a function of t_w at various ϕ's and U's. For a deep quench (Fig. 6), the scaled Δ and G' superimpose remarkably well at all ϕ's, thus linking unexpectedly precisely the gel's elastic properties to its microscopic dynamics.[65] For a shallower quench, the scaled parameters also superimpose closely, with no free parameters, at high ϕ's (Fig. 7b and c) but show a significant quantitative discrepancy at lower ϕ (Fig. 7a). This disparity between microscopic localization and macroscopic elasticity at low ϕ is not unexpected given that MCT is a mean-field-type theory that was more successful in describing depletion systems at higher particle ϕ.[66–68]

NMCT successfully connects the microscopic dynamics to the macroscopic mechanics of casein micelle gels. Furthermore, it applies to the t_w-dependence of gel localization and elasticity, despite it assuming quasi-steady state properties and hence not being suited for temporal evolution of gel formation and aging.[24] The extension of NMCT applicability, in depletion systems, from
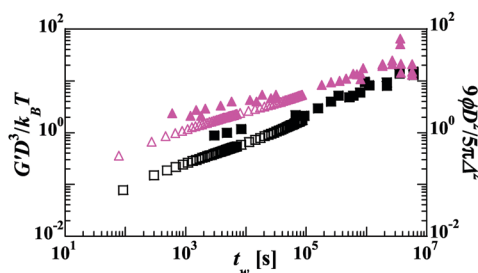

Fig. 6 Overlap of scaled shear modulus (open symbols) and localisation length (solid symbols) as a function of t_w for casein–PEO at a deep quench of $U \approx -13 \pm 0.5 k_B T$ and ϕ: 0.15 (black symbols), 0.2 (pink symbols). For clarity only data for two ϕ's are shown.
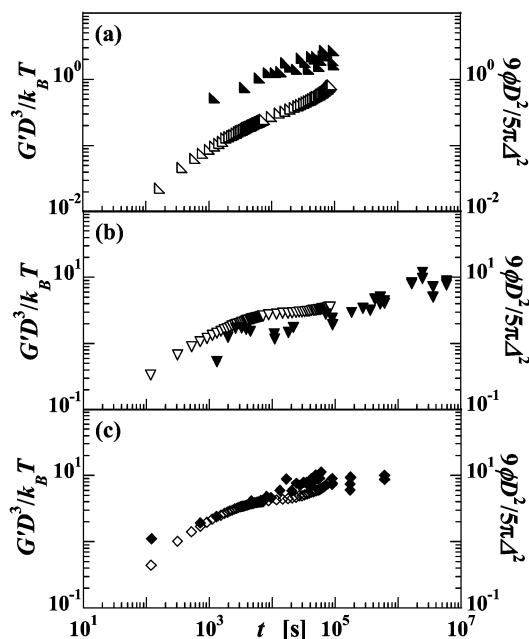
Fig. 7 Overlap of scaled shear modulus (open symbols) and localisation length (solid symbols) as a function of t_w for casein–PEO at $U \approx -9 \pm 0.5 k_B T$ and various ϕ: 0.15 (a), 0.25 (b) and 0.35 (c).

predicting the gel boundary and its steady-state properties,[66–68] to connecting localization and elasticity properties during gel temporal evolution is made possible because the timescales of casein localization (≈ 0.01 s, inset in Fig. 5) and its shear modulus ($\omega = 1$ rad s^{-1}) are considerably shorter than those characterizing the gel formation (t_a, Γ_g^{-1}).

Conclusions

We have examined the evolution of structural features, microscopic dynamics and macroscopic elastic moduli in a depletion bio-colloidal system undergoing gelation *via* arrested spinodal decomposition. Images of the microstructure show bicontinuous network of casein strands interlaced with particle-poor solvent regions, which form immediately after mixing ceases and show qualitatively no sign of coarsening. Absence of coarsening of the microstructure was confirmed by the time-independent l^* values, related to the structural properties of the network, from diffuse-transmission spectroscopy measurements. We have determined the structural arrest time from the macroscopic elastic properties during gel formation, and found that this characteristic time as well as the plateau modulus exhibit a power-law divergence as a function of ϕ and U, a scaling behaviour reminiscent of attractive colloidal gels and jammed systems in general. The gelation is associated with two-step-relaxation dynamics, a fast component in which a casein micelle diffuses within the restricted cage of its neighbours, and a slow component where it moves cooperatively away from its cage. This rich structural and dynamical behaviour of caseins at the microscopic level is intimately connected to macroscopic properties of gel formation. Naïve mode coupling theory successfully connects casein localization length, within its

neighbouring cage, to its elastic modulus during gel formation and aging.

We demonstrate that gelation *via* arrested spinodal decomposition in a polydisperse food protein system follows universal rules originally derived for simpler colloidal systems. The use of these theoretical concepts could aid understanding and hence improving more complex food mixtures.

Acknowledgements

Notes and references

1 E. Zaccarelli, *J. Phys.: Condens. Matter*, 2007, **19**, 323101.
2 J. C. Conrad, S. R. Ferreira, J. Yoshikawa, R. F. Shepherd, B. Y. Ahn and J. A. Lewis, *Curr. Opin. Colloid Interface Sci.*, 2011, **16**, 71–79.
3 M. N. Lee and A. Mohraz, *J. Am. Chem. Soc.*, 2011, **133**, 6945–6947.
4 R. Mezzenga and P. Fischer, *Rep. Prog. Phys.*, 2013, **76**, 046601.
5 M. Guvendiren, H. D. Lu and J. A. Burdick, *Soft Matter*, 2012, **8**, 260–272.
6 Z. Gu, A. A. Aimetti, Q. Wang, T. T. Dang, Y. Zhang, O. Veiseh, H. Cheng, R. S. Langer and D. G. Anderson, *ACS Nano*, 2013, **7**, 4194–4201.
7 V. J. Anderson and H. N. W. Lekkerkerker, *Nature*, 2002, **416**, 811–815.
8 W. C. K. Poon, *J. Phys.: Condens. Matter*, 2002, **14**, R859.
9 R. Mezzenga, P. Schurtenberger, A. Burbidge and M. Michel, *Nat. Mater.*, 2005, **4**, 729–740.
10 E. Dickinson, *Soft Matter*, 2006, **2**, 642–652.
11 M. Carpineti and M. Giglio, *Phys. Rev. Lett.*, 1992, **68**, 3327–3330.
12 P. N. Pusey and W. Van Megen, *Nature*, 1986, **320**, 340–342.
13 M. A. Miller and D. Frenkel, *Phys. Rev. Lett.*, 2003, **90**, 135702.
14 A. P. R. Eberle, R. Castañda-Priego, J. M. Kim and N. J. Wagner, *Langmuir*, 2012, **28**, 1866–1878.
15 M. E. Helgeson, S. E. Moran, H. Z. An and P. S. Doyle, *Nat. Mater.*, 2012, **11**, 344–352.
16 M. E. Helgeson, Y. Gao, S. E. Moran, J. Lee, M. Godfrin, A. Tripathi, A. Bose and P. S. Doyle, *Soft Matter*, 2014, **10**, 3122–3133.
17 L. C. Hsiao and P. S. Doyle, *Soft Matter*, 2015, **11**, 8426–8431.
18 S. Manley, H. M. Wyss, K. Miyazaki, J. C. Conrad, V. Trappe, L. J. Kaufman, D. R. Reichman and D. A. Weitz, *Phys. Rev. Lett.*, 2005, **95**, 238302.
19 S. Buzzaccaro, R. Rusconi and R. Piazza, *Phys. Rev. Lett.*, 2007, **99**, 098301.
20 R. N. Zia, B. J. Landrum and W. B. Russel, *J. Rheol.*, 2014, **58**, 1121–1157.
21 G. Foffi, C. De Michele, F. Sciortino and P. Tartaglia, *J. Chem. Phys.*, 2005, **122**, 224903.

22 E. Zaccarelli, P. J. Lu, F. Ciulla, D. A. Weitz and F. Sciortino, *J. Phys.: Condens. Matter*, 2008, **20**, 494242.

23 F. Cardinaux, T. Gibaud, A. Stradner and P. Schurtenberger, *Phys. Rev. Lett.*, 2007, **99**, 118301.

24 H. Guo, S. Ramakrishnan, J. L. Harden and R. L. Leheny, *J. Chem. Phys.*, 2011, **135**, 154903.

25 S. Ramakrishnan, M. Fuchs, K. S. Schweizer and C. F. Zukoski, *J. Chem. Phys.*, 2002, **116**, 2201–2212.

26 P. J. Lu, E. Zaccarelli, F. Ciulla, A. B. Schofield, F. Sciortino and D. A. Weitz, *Nature*, 2008, **453**, 499–503.

27 C. P. Royall, S. R. Williams, T. Ohtsuka and H. Tanaka, *Nat. Mater.*, 2008, **7**, 556–561.

28 L. J. Teece, M. A. Faers and P. Bartlett, *Soft Matter*, 2011, **7**, 1341–1351.

29 I. Zhang, C. P. Royall, M. A. Faers and P. Bartlett, *Soft Matter*, 2013, **9**, 2076–2084.

30 V. Testard, L. Berthier and W. Kob, *J. Chem. Phys.*, 2014, **140**, 164502.

31 J. C. Conrad, H. M. Wyss, V. Trappe, S. Manley, K. Miyazaki, L. J. Kaufman, A. B. Schofield, D. R. Reichman and D. A. Weitz, *J. Rheol.*, 2010, **54**, 421–438.

32 Y. Gao, J. Kim and M. E. Helgeson, *Soft Matter*, 2015, **11**, 6360–6370.

33 V. Testard, L. Berthier and W. Kob, *Phys. Rev. Lett.*, 2011, **106**, 125702.

34 S. W. Kamp and M. L. Kilfoil, *Soft Matter*, 2009, **5**, 2438–2447.

35 N. Koumakis and G. Petekidis, *Soft Matter*, 2011, **7**, 2456–2470.

36 P. Bartlett, L. J. Teece and M. A. Faers, *Phys. Rev. E: Stat., Nonlinear, Soft Matter Phys.*, 2012, **85**, 021404.

37 K. S. Schweizer and G. Yatsenko, *J. Chem. Phys.*, 2007, **127**, 164505.

38 N. Mahmoudi and A. Stradner, *J. Phys. Chem. B*, 2015, **119**, 15522–15529.

39 P. Zakharov, F. Cardinaux and F. Scheffold, *Phys. Rev. E: Stat., Nonlinear, Soft Matter Phys.*, 2006, **73**, 011413.

40 F. Scheffold, S. E. Skipetrov, S. Romer and P. Schurtenberger, *Phys. Rev. E: Stat., Nonlinear, Soft Matter Phys.*, 2001, **63**, 061404.

41 P. Hébraud, F. Lequeux, J. P. Munch and D. J. Pine, *Phys. Rev. Lett.*, 1997, **78**, 4657–4660.

42 A. S. Negi and C. O. Osuji, *J. Rheol.*, 2010, **54**, 943–958.

43 G. J. Fleer and R. Tuinier, *Adv. Colloid Interface Sci.*, 2008, **143**, 1–47.

44 P. D. Kaplan, A. D. Dinsmore, A. G. Yodh and D. J. Pine, *Phys. Rev. E: Stat., Nonlinear, Soft Matter Phys.*, 1994, **50**, 4827–4835.

45 S. Fraden and G. Maret, *Phys. Rev. Lett.*, 1990, **65**, 512–515.

46 M. Alexander, L. F. Rojas-Ochoa, M. Leser and P. Schurtenberger, *J. Colloid Interface Sci.*, 2002, **253**, 35–46.

47 A. Negi and C. Osuji, *Europhys. Lett.*, 2010, **90**, 28003.

48 F. Sciortino and P. Tartaglia, *Adv. Phys.*, 2005, **54**, 471–524.

49 C. J. Rueb and C. F. Zukoski, *J. Rheol.*, 1997, **41**, 197–218.

50 Y. Li, G. Wang and Z. Hu, *Macromolecules*, 1995, **28**, 4194–4197.

51 T. Gibaud and P. Schurtenberger, *J. Phys.: Condens. Matter*, 2009, **21**, 322201.

52 K. G. Soga, J. R. Melrose and R. C. Ball, *J. Chem. Phys.*, 1998, **108**, 6026–6032.

53 A. Furukawa and H. Tanaka, *Phys. Rev. Lett.*, 2010, **104**, 245702.

54 S. Bhat, R. Tuinier and P. Schurtenberger, *J. Phys.: Condens. Matter*, 2006, **18**, L339–L346.

55 V. Trappe, V. Prasad, L. Cipelletti, P. N. Segre and D. A. Weitz, *Nature*, 2001, **411**, 772–775.

56 V. Trappe and D. A. Weitz, *Phys. Rev. Lett.*, 2000, **85**, 449–452.

57 S. Ramakrishnan and C. F. Zukoski, *Langmuir*, 2006, **22**, 7833–7842.

58 A. S. Negi, C. G. Redmon, S. Ramakrishnan and C. O. Osuji, *J. Rheol.*, 2014, **58**, 1557–1579.

59 V. Prasad, V. Trappe, A. D. Dinsmore, P. N. Serge, L. Cipelletti and D. A. Weitz, *Faraday Discuss.*, 2003, **123**, 1–12.

60 L. F. Rojas, R. Vavrin, C. Urban, J. Kohlbrecher, A. Stradner, F. Scheffold and P. Schurtenberger, *Faraday Discuss.*, 2003, **123**, 385–400.

61 A. H. Krall and D. A. Weitz, *Phys. Rev. Lett.*, 1998, **80**, 778.

62 S. Romer, F. Scheffold and P. Schurtenberger, *Phys. Rev. Lett.*, 2000, **85**, 4980.

63 S. Reuveni, J. Klafter and R. Granek, *Phys. Rev. Lett.*, 2012, **108**, 068101.

64 S. Romer, H. Bissig, P. Schurtenberger and F. Scheffold, *Europhys. Lett.*, 2014, **108**, 48006.

65 Y. L. Chen and K. S. Schweizer, *J. Chem. Phys.*, 2004, **120**, 7212–7222.

66 S. A. Shah, Y. L. Chen, K. S. Schweizer and C. F. Zukoski, *J. Chem. Phys.*, 2003, **119**, 8747–8760.

67 S. Ramakrishnan, Y. L. Chen, K. S. Schweizer and C. F. Zukoski, *Phys. Rev. E: Stat., Nonlinear, Soft Matter Phys.*, 2004, **70**, 040401.

68 S. Ramakrishnan, V. Gopalakrishnan and C. F. Zukoski, *Langmuir*, 2005, **21**, 9917–9925.